Applied Catalysis B: Environmental 144 (2014) 46–56

Contents lists available at ScienceDirect

Applied Catalysis B: Environmental

journal homepage: www.elsevier.com/locate/apcatb

# Aldol-condensation of furfural by activated dolomite catalyst

Rebecca E. O'Neill[a], Laurent Vanoye[b], Claude De Bellefon[b], Farid Aiouache[c,*]

[a] Queen's University Belfast, School of Chemistry and Chemical Engineering, Stranmillis Road, Belfast BT9 5AG, Ireland
[b] Laboratoire de Génie des Procédés Catalytiques (LGPC), UMR 5285 CNRS/CPE Lyon, Université de Lyon, 43 boulevard du 11 novembre 1918, 69616 Villeurbanne Cedex, France
[c] Lancaster University, Engineering Department, LA1 4YR Lancaster, United Kingdom

ARTICLE INFO

*Article history:*
Received 21 March 2013
Received in revised form 11 June 2013
Accepted 2 July 2013
Available online 11 July 2013

*Keywords:*
Basic catalysis
Aldol-condensation
Kinetics and mechanism
Dolomite
Mixed oxide catalysts

ABSTRACT

Aldol-condensation of furfural with acetone catalysed by activated dolomite was investigated at temperatures from 306 to 413 K. The process of activation by calcination and hydration produced catalytically active calcium and magnesium hydroxides with improved surface area and surface basicity. The aldol-condensation mechanism began with a deprotonation of acetone forming a carbanion intermediate by hydroxyl ions, which then reacted with the carbonyl group of furfural to form a water soluble $C_8$ monomer (4-(furan-2-yl)-4-hydroxybutan-2-one). This $C_8$ monomer readily dehydrated to form selectively α,β-unsaturated ketone (4-(2-furyl)-3-buten-2-one), which in turn, reacted with furfural forming a $C_{13}$ dimer (1,4-pentadien-3-one,1,5-di-2-furanyl). Compared with conventional sodium hydroxide catalyst, activated dolomite was less selective towards lumped $C_8$ monomers and $C_{13}$ dimers owing to carbon losses and deactivation, particularly at high temperatures. Activated dolomite was more selective to $C_{13}$ dimer owing to higher adsorption enthalpy of $C_8$ monomer compared with acetone competitor. Activated dolomite is therefore a promising catalyst to produce $C_{13}$ dimers which can be transformed upon hydrogenation and deep hydrodeoxygenation in high-quality diesel fuels. The first-order kinetic model with respect to furfural and acetone fitted well with actual experimental results with an average normalised standard deviation of 6.2%.



## 1. Introduction

The development of usable renewable energy is a major challenge in the twenty-first century owing to the finite nature of fossil fuels and their environmentally damaging effects. Burning of fossil fuels, for instance, is the anthropogenic activity which contributes the most to increasing levels of carbon dioxide in the atmosphere with an inevitable consequence on global warming [1]. Bio-refineries are cited as a good option to respond to humanity's concerns about sustainable energy as they integrate multiple biomass conversion processes to produce fuels, power, heat, and value added chemicals, with reduced waste and energy usage [2]. The key goal of a bio-refinery process is to transform this captured energy into usable energy. Liquid fuels represented by bio-alkanes have been synthesised by the hydrodeoxygenation of sugar derivatives which comprises dehydration of associated aldehydes, followed by hydrogenation and condensation to produce long chain alkanes [3]. It has previously been shown that furfural can be produced from xylose with high yields using aqueous phase dehydration [4]. Furfural is a highly versatile intermediate which can be transformed into a variety of chemicals by hydrogenation, oxidation, reductive amination, decarbonylation, nitration and condensation. Processes of aldol-condensation, hydrogenation and hydrodeoxygenation are seen as effective integration steps towards the production chain of liquid fuels and industrial production is anticipated [4–9].

The reaction of aldol-condensation is base catalysed, bonds two carbon molecules together to produce longer hydrocarbon chains and ultimately produces low volatile and easy to transport fuels. Base catalysed aldol-condensation proceeds through a nucleophilic attack of the enolate ion on the $C^{\delta+}$ atom of the C=O group [6,10–12]. The reaction may occur between two ketones, two aldehydes or an aldehyde and a ketone, provided that one member of each pair possesses an α-H-atom. The missing α-H-atom in furfural does not allow, therefore, its self-condensation. As shown in Fig. 1, a proton is abstracted from the α-carbon, herein the acetone carbonyl function, creating a carbanion and leading to the formation of $C_8$ monomer, 4-(2-furyl)-3-buten-2-one (FAc). Due to the symmetry of the acetone molecule, the FAc monomer is, in turn, susceptible to a second attack by furfural leading to a double condensation $C_{13}$ dimer, 1,4-pentadien-3-one,1,5-di-2-furanyl (FFAc) [7]. Fakhfakh et al. [8] successfully used sodium hydroxide to catalyse the aldol-condensation reaction of furfural and acetone at temperatures between 293 and 313 K in homogeneous

* Corresponding author. Tel.: +44 01524593526; fax: +44 01524593526.
*E-mail address:* f.aiouache@lancaster.ac.uk (F. Aiouache).

0926-3373/$ – see front matter © 2013 Elsevier B.V. All rights reserved.
http://dx.doi.org/10.1016/j.apcatb.2013.07.006

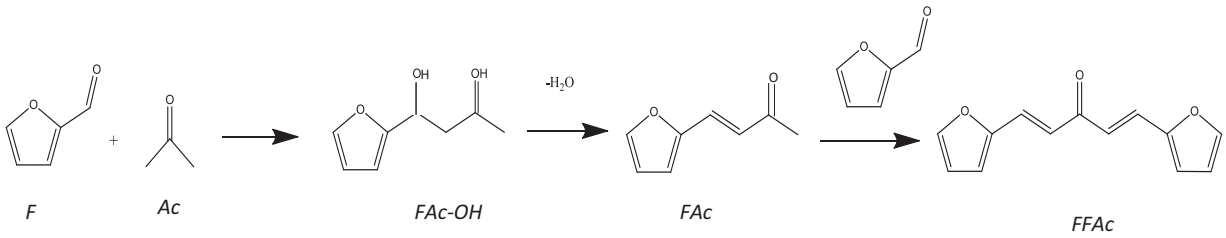


**Fig. 1.** Proposed reaction pathway for aldol-condensation of furfural with acetone. *F*: Furfural, *Ac*: Acetone, *FAc-OH*: 4-(furan-2-yl)-4-hydroxybutan-2-one, *FAc*: 4-(2-furyl)-3-buten-2-one and *FFAc*: 1,4-pentadien-3-one,1,5-di-2-furanyl [7].

ethanol–water solvent. Yields of around 50% were achieved. Similarly, West et al. [9] investigated aldol-condensation using biomass derived furans such as furfural, methyl furfural and HMF along with ketones such as acetone, acetol, dihydroxyacetone, 2-hexanone and 3-hexanone. A reactive aqueous phase was used including a homogeneous base NaOH catalyst and a salt in a biphasic system to reach high product yields by phase transfer separation. Although sodium hydroxide is a cost effective base, it completely dissociates in water and raises therefore some downstream processing issues such as energy intensive separation, product neutralisation, waste disposal and potential regeneration [10–19]. Recently, there has been a shift towards heterogeneous base catalysts such as alkali and alkaline earth oxides, phosphates and molecular sieves, i.e. mobile crystalline material (MCM-41) and hydrotalcites. Guida et al. [20] who investigated the Claisien-Schmidt condensation of benzaldehyde with excess acetone using calcined hydrotalcites as catalyst, recognised the catalytic effect of basic hydroxyls. Uncalcined hydrotalcites were initially found to be totally inactive, but once thermally treated and hydrated, were found to be active, implying that the reaction was catalysed specifically by hydroxyl sites. Yoosuk et al. [21] used activated dolomite as heterogeneous catalyst for the reaction of palm oil transesterification with methanol. The most effective catalyst was the dolomite sample which was subject to calcination, hydration and second calcination. The initial calcination transformed the non-porous structure of natural dolomite to a mesoporous structure of CaO–MgO resulting from the expulsion of carbon dioxide from the dolomite's core. Upon exposure to water, the oxide part became swollen and was transformed to a hydroxide surface. Upon a second calcination, the hydroxide structure was reversed back to an oxide coincident with the release of a molecule of water, the production of a higher surface area along with a lower crystalline size. After hydration–dehydration, the strong basic sites were considerably enhanced. Wilson et al. [22] used dolomite for transesterification of $C_4$ and $C_8$ triglycerides and olive oil for biodiesel applications. The active sites were thought to be the calcium oxide portion of the dolomite which was produced by calcination and decomposition of the dolomite structure.

The aim of this work is to investigate the aldol-condensation of furfural with acetone at relatively low temperatures using calcined and hydrated dolomite as base catalyst. Dolomite was selected because it presents high green credentials owing to its abundance and low toxicity [21]. Dolomite is an abundant sedimentary carbonate rock containing alternating plane structures of $Ca^{2+}$ and $Mg^{2+}$ cations forming a non-ideal chemical composition of basic $CaMg(CO_3)_2$. The work focuses on experimental validation of the mechanism involved in a monophasic system. An activated dolomite by calcination and fully hydration is used as it offers a constant number of fully developed Brønsted hydroxyl sites for the kinetic modelling. These hydroxyl sites were found more effective than relevant Lewis sites of mixed oxides [10–18,23]. The kinetic modelling of furfural as biomass derivative compound model provides a promising option to produce, under controlled operating conditions, the desired route towards product oxygenates FAc monomer, 1,4-pentadien-3-one or FFAc dimer which are sources of the desired alkanes in bio-refinery processing. A reaction mechanism is proposed and the kinetic parameters normalised to hydroxyl base sites are estimated and compared with those of sodium hydroxide catalyst.

## 2. Experimental

### 2.1. Catalyst preparation and characterisation

A natural dolomitic rock was mined from a deposit in Fermanagh, (Northern Ireland), ground on site and supplied in its powdered and brownish form. Dolomite was calcined in air using a tubular furnace at 1073 K. A range of methods were used to characterise the chemical and structural changes occurring within the dolomite. The basicity strength of dolomite was carried out by Hammett indicators (bromothymol blue, phenolphthalein, and 2,4-dinitroaniline) in anhydrous methanol and volumetric titration using acetic acid. X-ray diffraction (XRD) analysis was performed using a PANalytical X'Pert Pro X-Ray Diffractometer with Cu $K_\alpha$ radiation. The $2\theta$ range was scanned between angles of 5° and 60° and the detector was set at 40 kV and 40 mA. Scanning electron microscopy (SEM) was carried out using a Jeol JSM-6500F Field Emission working at 0.5–30 kV and giving a resolution of 1.5 nm. The surface area analysis was carried out using a BET Micromeritics ASAP 2010. Thermogravimetric analysis was carried out using Mettler Toledo using a 5 mg dolomite sample that was heated to a temperature of 1273 K. Spent dolomite was analysed by temperature-programmed desorption (TPD) using Krypton as reference gas and temperature-programmed oxidation (TPO) using a mixture of krypton, argon and oxygen (40:50:10 mol.%), at a heating rate of 5 K/min. Soluble dolomite ions in water were analysed by inductively coupled plasma/atomic emission spectrometer (ICP/AES).

### 2.2. Batch reactor

The reactor was a 316 L stainless steel, 100 mL four ports Parr reactor. An on/off controlled heating jacket was used ensuring a liquid phase temperature within a 2 K deviation from the set-point. The heating jacket and the agitator were controlled using an Autoclave Engineers Sentinel Series control box. A sampling valve was attached to a threaded piece of 1/8 in. tubing that was immersed inside the liquid phase of the reactor. The reactor also included a 50 mL stainless steel sampling vessel which was connected to a supply of helium at 20 bars pressure. This additional setup allowed furfural to be held at room temperature and charged to the reactor at the desired temperature. This procedure minimised degradation of furfural before the start of the reaction.

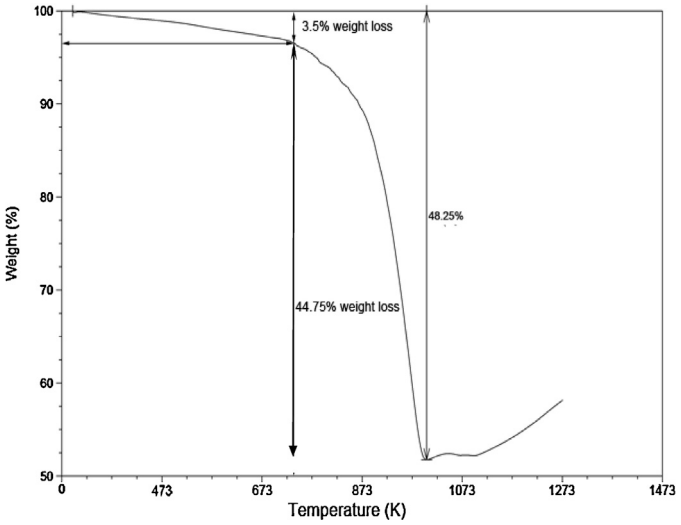


**Fig. 2.** Thermo-gravimetric analysis of dolomite rock sample, 5 mg of dolomite and heating rate at 50 K/min from ambient temperature to 1273 K.

### 2.3. Procedure

The following amounts were used: 3.3 g of acetone (Sigma Aldrich, 99.9% purity), 5.5 g of furfural (Sigma Aldrich, 99% purity) in equimolar with acetone, and 0.5 g of calcined and hydrated dolomite in 60 g of solvent (1:1.5 weight ratio (w/w) of water to methanol (Sigma Aldrich, 99.8% purity)). Methanol was used to carry out the reaction in a monophasic medium by promoting the solubility of furfural and its condensation derivatives in water. The hydration of calcined dolomite was carried out in liquid water for 2 h at the desired reaction temperature using the same reactor for kinetic tests. This time was sufficient to reach the highest conversion of CaO and MgO into $Ca(OH)_2$ and $Mg(OH)_2$, respectively. The catalyst, along with the solvent mixture, was placed in the reactor which was then purged and pressurised to 20 bars by helium ensuring a liquid phase under an inert atmosphere. At typical operations, the mixture of methanol, water and activated dolomite was stirred at 1200 rpm and the reactants were then forced into the reactor using helium pressure. Initial samples were taken every minute and less frequently as the reaction continued. The samples were filtered and analysed by gas chromatography. A Perkin Elmer 500 gas chromatogram fitted with a DB-5 column was used. The oven was heated to 40 °C for 2 min before being ramped up at a rate of 40 °C/min to 300 °C. The reactants and products were identified by gas chromatography coupled to a mass-spectroscopy detector (GC–MS) and confirmed by conventional internal standard methods.

## 3. Results and discussion

### 3.1. Catalyst characterisation

The thermal stability and composition of dolomite were investigated by calcination or charring at temperatures above 873 K for an extended period of time using TGA as shown in Fig. 2. The decomposition occurred at temperatures ranging from 873 to 1173 K by releasing carbon dioxide. The TGA profile shows a small weight loss (ca. wt. 3.5%) until 773 K, followed by a significant weight loss at around 1073 K. The following reactions take place.

$$CaMg(CO_3)_2 \rightarrow CaCO_3 + MgO + CO_2 \quad (1)$$

$$CaCO_3 \rightarrow CaO + CO_2 \quad (2)$$

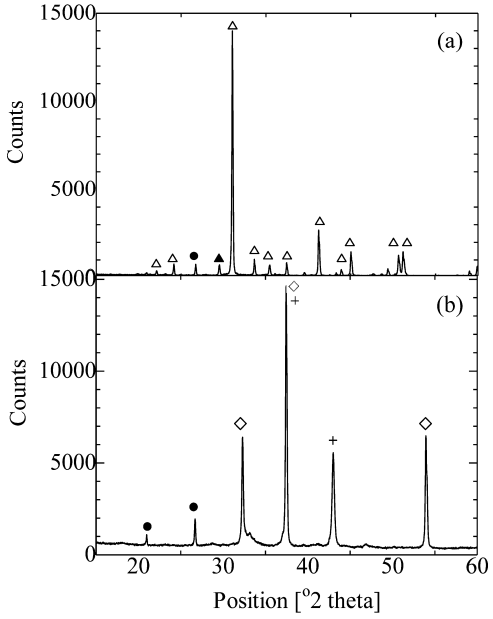


**Fig. 3.** X-ray diffraction of (a) fresh dolomite (△ – dolomite, ▲ – calcite, ● – quartz). (b) calcined dolomite (◊ – calcium oxide, + – magnesium oxide, ● – quartz).

The first step, which occurred at 873–973 K, would involve the decomposition of the magnesium fraction of dolomite. Magnesium carbonate would break down releasing carbon dioxide and powdered magnesium oxide dispersed over a rigid porous calcite. Upon further heating (1073 K and above), the structure would decompose further with the calcite fraction leaving calcium oxide. The evolution of carbon dioxide from the dolomite structure would cause an increase in dolomite porosity and surface area [24]. The cumulated weight loss at the intermediate temperature of 1072 K (originating form magnesium oxide only) was 45.0% which is slightly lower than the theoretical value of 52.2% implying that the dolomite used was slightly rich in calcite with a potential composition of $Ca_{1.25}Mg(CO_3)_{2.25}$.

The crystallinity of dolomite before and after the thermal treatment was probed by XRD analysis. Fig. 3a illustrates the patterns of the raw powdered dolomite. The main diffraction peak occurs at $2\theta = 31$ which is characteristic of the reflection of dolomite. The smaller peak which diffracts at $2\theta = 29$ is characteristic of the crystalline peak for calcite in agreement with the results of Duffy et al. [25]. It is interesting to note that the presence of calcite here is in agreement with the results of the TGA where the dolomite used was found to be slightly calcite rich. The weaker reflections which can be seen between $2\theta = 35$ and 55 are also consistent with the presence of both dolomite and calcite. The small peak at $2\theta = 27$ confirms the presence of quartz impurities, which is quite common in natural dolomite [26]. The XRD analysis of the dolomite sample which has been calcined for 8 h is illustrated in Fig. 3b. The sample is different from that of the parent dolomite. Reflections arising from dolomite and calcite disappeared and were replaced by new crystalline phases, the most prominent of which can be assigned to calcium oxide as shown by the diffraction peaks at $2\theta = 32$, 37 and 54. The second peak at $2\theta = 37$ along with the smaller peak at $2\theta = 43$ are consistent with the presence of magnesium oxide [23]. Such close characteristics peaks suggest some synergy between the two phases of calcium and magnesium oxides.

From this data, it can be concluded that calcining dolomite at 1073 K for 8 h is sufficient to cause complete decomposition of the structure. If only partial decomposition had occurred, the calcined sample would have displayed calcite and dolomite diffraction peaks, along with the magnesium oxide peak. The lack of any trace

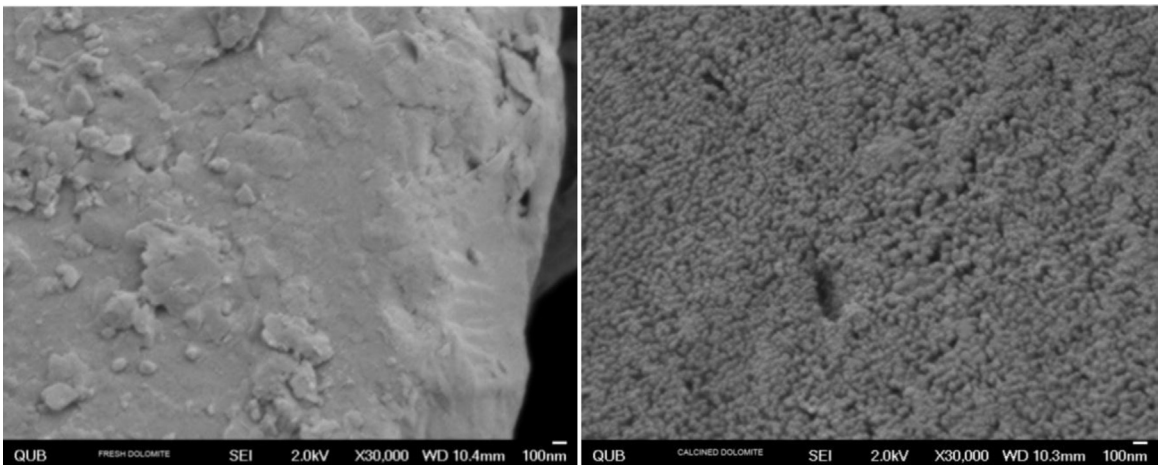


**Fig. 4.** Scanning electron micrographs of fresh (right) and calcined (left) dolomite samples.

of either dolomite or calcite peaks at post-calcination implies that dolomite [$CaMg(CO_3)_2$] has broken down into its calcium oxide (CaO) and magnesium oxide (MgO) components whilst carbon dioxide has been released from the structure. These changes are reflected by the SEM images as shown in Fig. 4, which very clearly demonstrate the profound effect of charring on the dolomite surface by causing a notable change in the surface topography where the nonporous structure of the non-calcined sample has been transformed into a mesoporous one. This is in agreement with the work of Yoosuk et al. [21] where newly created pores and slots are clearly visible and which can be attributed to the release of carbon dioxide leaving gaps within the structure and contributing to the roughness of the dolomite surface. The angular, smooth planes have been replaced by a porous, almost sponge like surface texture. This result is also in agreement with the BET results, as shown in the following section, where the calcination has been found to contribute to both the porosity and the surface area of dolomite.

As the reaction takes place in the aqueous phase, the effect of water on the structure of the calcined dolomite was analysed using BET and XRD. The adsorption isotherms of $N_2$ on dolomite in natural, calcined and hydrated forms are shown in Fig. 5 (a)–(c). The hydrated form of dolomite was sampled after 15 min of hydration time and 333 K. The isotherm of the natural dolomite in Fig. 5(a) follows isotherms of type III and illustrates a continuous increase in volume of adsorbed gas by formation of multiple layers on a non-porous dolomite. Isotherms of calcined and hydrated dolomites in Fig. 5(b) and (c) show typical isotherms of type IV for mesoporous materials, where the porous volume increased from 0.009 $cm^3\,g^{-1}$ in the natural dolomite to 0.09 $cm^3\,g^{-1}$ for the calcined dolomite and 0.23 $cm^3\,g^{-1}$ for the hydrated dolomite. The surface area of natural dolomite increased from 3.2 to 12.3 $m^2/g$ after calcination, and 25 $m^2/g$ after hydration. The averaged pore size of dolomite increased from 3.2 to 10.5 nm after calcination and increased further to 13.5 nm after hydration. The substantial increase of the porous volume compared with the pore size produced is well justified by observed type I hysteresis in isotherms of calcined and hydrated dolomites suggesting a uniform array of pore size distribution which was developed without pore networking. This volume increase allowed hydroxyl sites to be more accessible since surface basicity of calcined dolomite increased from 0.31 to 0.72 meq. $OH^-/g$ after hydration as illustrated in Table 1. Most of the generated basic sites were of medium strength confirming their effectiveness for single and double condensation reactions [8]. The structure of calcined and hydrated dolomite was also investigated by XRD analysis. Partial hydrolysis of calcium oxide to calcium hydroxide and negligible hydrolysis of magnesium oxide to magnesium hydroxide were achieved after 15 min of hydration time as shown in Fig. 6. The calcium oxide diffraction peaks which were previously seen at $2\theta = 32$, 37 and 54 were significantly smaller and were replaced by a large peak at $2\theta = 29$ and 34. These peaks confirm the presence of calcium hydroxide.

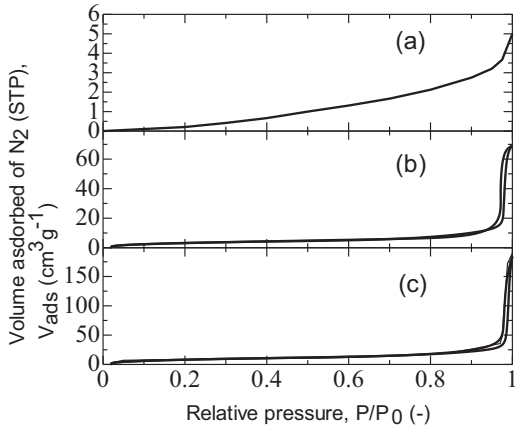


**Fig. 5.** Adsorption isotherms of $N_2$ on (a) natural, (b) calcined and (c) hydrated dolomites (hydration time: 15 min and temperature: 333 K).

### 3.2. Liquid phase profile

Liquid samples which were identified by gas chromatography were FAc monomer, FFAc dimer and 4-(furan-2-yl)-4-hydroxybutan-2-one monomer (FAc-OH). The evolutions of

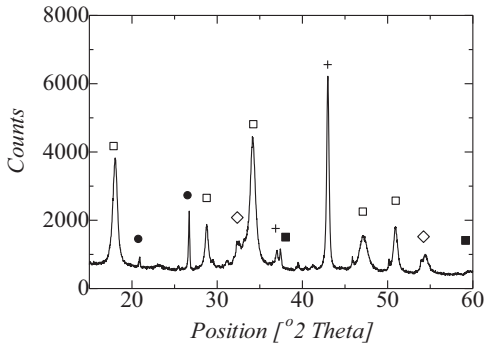


**Fig. 6.** X-ray diffraction of calcined hydrated dolomite (◊ – calcium oxide, + – magnesium oxide, □ – calcium hydroxide,■- – magnesium hydroxide ● – quartz). Hydration time: 15 min, temperature 333 K.

**Table 1**
Basicity of calcined and hydrated dolomites.

| Dolomite state | Basicity (meq. $OH^-$/g) $H_- = 7.2–9.8$ | Basicity (meq. $OH^-$/g) $H_- = 9.8–15.0$ | Total basicity (meq. $OH^-$/g) |
|---|---|---|---|
| Calcined | 0.14 | 0.17 | 0.31 ± 0.05 |
| Calcined and hydrated at 413 K | 0.17 | 0.55 | 0.72 ± 0.05 |
| Calcined and *in situ* hydrated at 413 K | 0.11 | 0.49 | 0.60 ± 0.05 |

reactants and products along with the reaction course at 323 K are shown in Fig. 7 for both activated dolomite and sodium hydroxide catalysts. Sodium hydroxide has been successfully used as base catalyst for aldol-condensation reactions [9,10] and exhibits a complete dissociation in water avoiding mass transfer and adsorption limitations. In case of activated dolomite, the pH of the system was monitored throughout the reaction and was found constant suggesting that no leaching or surface change distribution of Brønsted base sites. ICP analysis of the liquid phase collected from reaction test at 323 K showed traces of $Mg^{+2}$ (0.036 mg/L) or 0.02 wt.% loss in $Mg(OH)_2$ part of dolomite and a concentration of $Ca^{+2}$ of 1.6 mg/L or 1.4 wt.% loss in $Ca(OH)_2$ part of dolomite. Aldol condensation was mainly catalysed by the solid dolomite with negligible kinetic effect of the dissolved base sites. These profiles support the reaction scheme proposed by Fakhfakh et al. [8] as shown in Fig. 8 which was extended to FFAc.

The presence of the Brønsted base would induce the abstraction of a proton from the α-group of acetone carbonyl and form a carbanion (step 1). This would then condense on the carbon of the furfural carbonyl function, leave an oxyanion (step 2) and fix to a proton forming FAc-OH (step 3). This step is followed by dehydration in the basic medium which would regenerate the hydroxyl ion and form FAc (steps 4 and 5). The re-condensation of FAc to FFAc follows similar steps: abstraction of a proton from the α-group of FFAc carbonyl, condensation on the carbon of furfural carbonyl (step 6), condensation on the carbon of furfural carbonyl, fixation to a proton and dehydration into FFAc (steps 7–9).

The profiles show an immediate decrease of acetone and furfural, which initially decreased at a similar rate as FAc-OH was evolved. FAc-OH quickly disappeared as it dehydrated to form FAc. The acetone and furfural concentrations then diverged from each other; the rate of acetone disappearance slowed as the acetone concentration levelled off whilst the rate of disappearance of furfural continued. The rate of evolution of FAc shows that FAc and furfural were reacting to produce FFAc. One molecule of furfural reacted with one molecule of acetone to produce FAc and then went on to react with FAc forming FFAc while the disappearance of acetone slowed. The fact that FAc-OH appeared first, followed by FAc and finally FFAc would imply that the reactions take place consecutively, as suggested by Sadaba et al. [7]. It may be noted that despite the condensation reaction between FAc and furfural being chemically identical to the condensation reaction between acetone and furfural due to the symmetry of the acetone molecule, no intermediate hydrated molecule is seen in this case. In

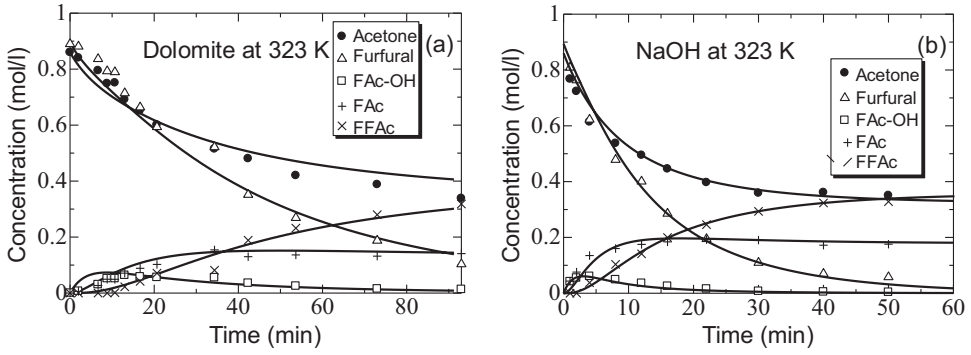


**Fig. 7.** Liquid reaction profile for aldol-condensation of furfural with acetone at 323 K, (3.3 g acetone, 5.5 g furfural and 60 g of 1:1.5 (w/w) water and methanol solvent mixture); (a) 0.5 g activated dolomite and (b) 0.02 mol/l of NaOH.

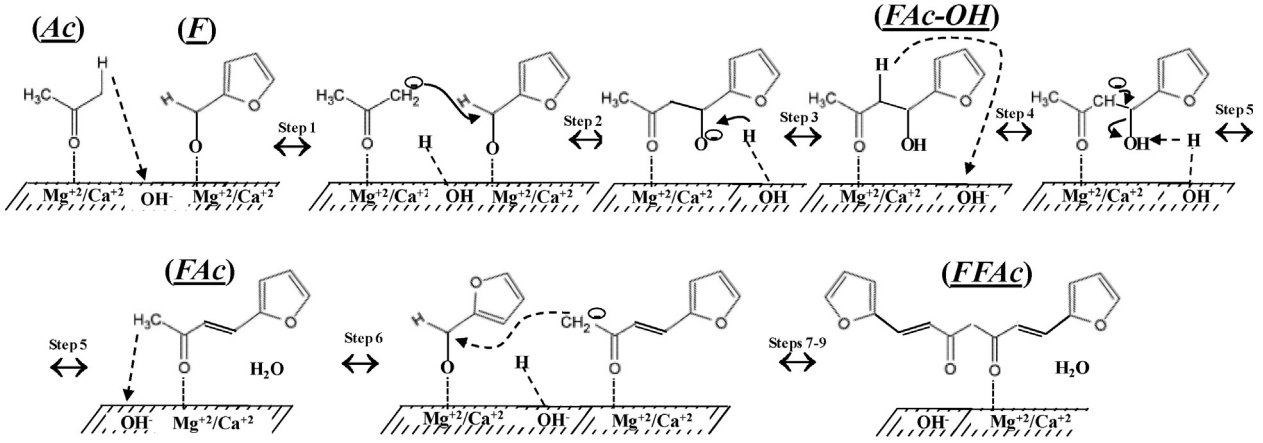


**Fig. 8.** Reaction scheme for aldol-condensation of acetone and furfural, steps 7–9 include condensation on the carbon of furfural carbonyl (step 7), fixation to a proton (step 8) and dehydration into FFAc (step 9).

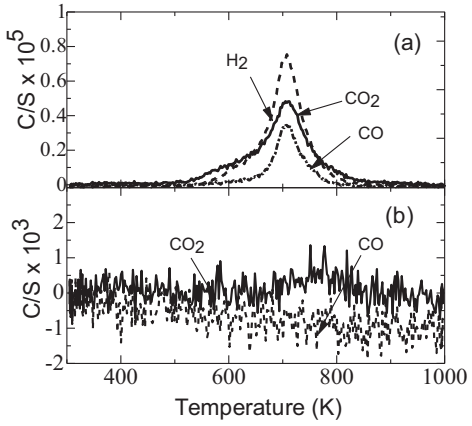


**Fig. 9.** TPD/TPO profiles of spent dolomite catalyst at 413 K (a) TPD and (b) TPO.

addition, side reactions of esterification of furfural to 2-furancarboxylic 2-furanmethyl ester ($C_{10}$) in organic-aqueous biphasic systems through furoic acid and furfuryl alcohol disproponations were not observed [26]. The carbon balance profiles as expressed by Eq. (3) at temperatures of 306, 323, 343, 373 and 413 K for activated dolomite catalyst and 293, 323 and 343 K for NaOH catalysts are shown in the supplementary Fig. S1(a) and (b), respectively [26].

$$\text{Carbon balance} = \frac{3C_{Ac} + 5C_F + 8C_{FAc\text{-}OH} + 8C_{FAc} + 13C_{FFAc}}{3C^0_{Ac} + 5C^0_F} \quad (3)$$

Herein, $C$ is the concentration in the liquid phase and $C^0$ is the initial concentration. The losses in terms of carbon balance did not exceed 5% for activated dolomite in all experiments and were negligible at low temperatures. At high temperatures, an average carbon loss of 5% was observed after 20 min of reaction progress (cf. furfural conversion of 0.6 in Fig. 10). Losses at high temperatures would be associated with deposits on activated dolomite of long chain furfural oligomers [4,27–31]. Theses losses were however a magnitude higher than those found in NaOH catalyst tests (Fig. S1(b)) demonstrating that NaOH was more selective towards the first and second condensations of furfural.

### 3.3. Reutilisation of activated dolomite

In addition to the selectivity towards the first and second condensations, the reusability of activated dolomite catalyst is another critical factor for comparison with the cost-effective sodium hydroxide. Since the highest temperatures have shown the highest losses in carbon with activated dolomite, a spend catalyst collected from the run at 413 K was first examined for reusability. This test was conducted by cooling, filtering, washing with water and re-running the test with fresh furfural, acetone and solvent mixture (water and methanol). The spent dolomite took a sludge-like brown appearance with a drop in the surface basicity to 0.23 meq. $OH^-$/g. In addition, the TPD and TPO results in Fig. 9(a) and (b) show that $H_2$ was released at the same temperature (773 K) as $CO_2$; therefore they were bound together for the formation of carbonates [26] at the surface of the catalyst. Further TPO test shows no significant $CO_2$ peaks, so all surface carbonates were released as $CO_2$ during the TPD experiment and were not tightly bound to the surface. Furthermore, supplementary Fig. S2 shows a large drop in furfural conversion after the recycle (10% vs. 80% of fresh catalyst). It should be noted that the recycled dolomite was not completely regenerated as further calcination to remove the carbonaceous deposits followed by rehydration could change the surface structure [21]. The tests on catalyst deactivation were then extended to all temperatures where the liquid phase was analysed by ICP to follow potential leaching of dolomite base sites. The separation of spent catalysts was carried out in inert atmosphere to avoid $CO_2$ contamination. The recycle of spent catalyst at 413 K required an additional de-carbonation by calcination at 1000 K. The results of four successive recycles exhibited a deactivation coefficient of 92–96% after each recycle of spent catalysts as shown in Table S3 (supplementary material), catalyst particles of unchanged size and weight losses of $Mg^{+2}$ and $Ca^{+2}$ of 0.01–0.03 and 0.86–2.53%, respectively. It is interesting to see that the spent catalyst at 413 K is exhibiting the lowest deactivation suggesting more porosity after expulsion of water during the de-carbonation process. The trends of this weak deactivation followed well those of base site dissolution suggesting that the weak deactivation at low temperature was driven by catalyst leaching and the strong deactivation at high temperature was driven by carbon deposits. These results agree with Faba's data [26] where the deactivation was assigned to structural changes of oxide catalysts and carboneous deposits rather than metal lixiviation.

### 3.4. Reaction mechanism and kinetics

Directed by preliminary experiments on activated dolomite illustrated in supplementary Fig. S4, the resistance to external mass transport was reduced by setting the speed of the agitator to 1200 rpm. The internal mass transport was considered negligible as a small particle size of an average diameter of 13 μm was used. The mechanism illustrated in Fig. 8 is summarised as follows:

$$Ac + * \leftrightarrow Ac* \quad (4a)$$

$$Ac* + OH^-* \leftrightarrow Ac^-* + water* \quad (4b)$$

$$F + * \leftrightarrow F* \quad (4c)$$

$$Ac^-* + F* + water* \leftrightarrow FAc - OH* + OH^-* + * \quad (4d)$$

$$FAc - OH* + OH^-* \leftrightarrow FAc - OH^-* + water* \quad (4e)$$

$$FAc - OH^-* + * \leftrightarrow FAc* + OH^-* \quad (4f)$$

$$FAc* + OH^-* \leftrightarrow FAc^-* + water* \quad (4g)$$

$$FAc^-* + F* \leftrightarrow FFAc* + OH^-* \quad (4h)$$

$$water* \leftrightarrow water + * \quad (4i)$$

$$FAc* \leftrightarrow FAc + * \quad (4j)$$

$$FFAc* \leftrightarrow FFAc + * \quad (4k)$$

where "*" represents a surface active site (metal cation or Brønsted hydroxyl anions). Assuming a relevance of surface kinetic steps over adsorption and desorption sequences and quasi-steady state for carbanion intermediates, Eqs. (4a)–(4k) are summarised as follows:

$$F + Ac \leftrightarrow FAc\text{-}OH \quad (5a)$$

$$FAc\text{-}OH \leftrightarrow FAc + water \quad (5b)$$

$$FAc + F \leftrightarrow FFAc + water \quad (5c)$$

Profiles of conversion (Eq. (6a)) and product yield (Eqs. (6b)–(6d)) profiles were analysed with reference to the limiting

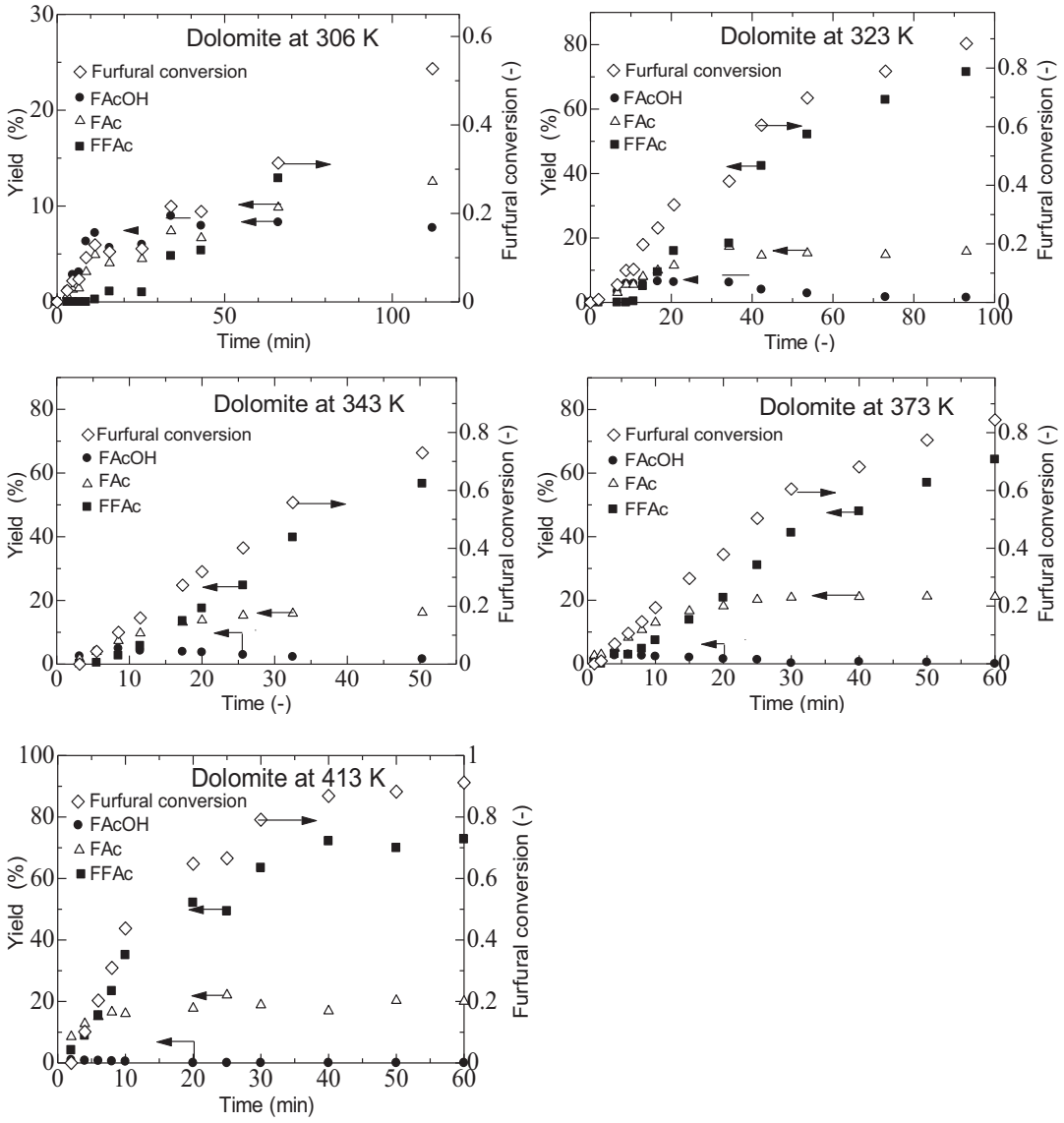


**Fig. 10.** Product yield and furfural conversion profiles with dolomite catalyst at 306, 323, 343, 373 and 413 K, (3.3 g acetone, 5.5 g furfural, 0.5 g activated dolomite, and 60 g of 1:1.5 (w/w) water and methanol solvent mixture).

reactant, furfural, which is involved in two reactions (5a) and (5c) compared with acetone.

$$\text{Conversion} = \frac{C_F^0 - C_F}{C_F^0} \tag{6a}$$

$$\text{Yield}_{\text{FAc-OH}}(\%) = \frac{C_{\text{FAc-OH}}}{C_F^0} \times 100 \tag{6b}$$

$$\text{Yield}_{\text{FAc}}(\%) = \frac{C_{\text{FAc}}}{C_F^0} \times 100 \tag{6c}$$

$$\text{Yield}_{\text{FFAc}}(\%) = \frac{2C_{\text{FFAc}}}{C_F^0} \times 100 \tag{6d}$$

### 3.4.1. *Effect of temperature*

The reaction was carried out using activated dolomite at temperatures ranging from 306 K to 413 K and NaOH at temperatures from 293 to 343 K as shown in Fig. 10(a)–(e) and Fig. 11(a)–(c), respectively. Increasing the temperature favoured the dehydration step as shown by the decrease in yield of FAc-OH from 7.4 to 0.1% when temperature was increased from 306 to 413 K with activated dolomite and from 10.7 to 2.4% when temperature was increased from 293 to 343 K with NaOH catalyst. The maximum yields of FAc and FFAc with activated dolomite were 12.6 and 32.4% after 60 min at a temperature of 306 K, respectively, and increased to 15.8 and 60.0% at 323 K (i.e. furfural conversion of 0.75). In case of NaOH catalyst, maximum yields of FAc and FFAc at furfural conversion of 0.75 were 21.6 and 55.3%, respectively. These results show that temperatures promoted the selectivity of activated dolomite catalyst into the re-condensation step for FFAc and activated dolomite was more selective towards FFAc (the second condensation) than NaOH, although the later was more selective towards both condensation and re-condensation as shown by the carbon losses. A maximum yield of 72.8% at 423 K using activated dolomite is comparable with yields obtained by Faba et al. [26] using Mg–Zr mixed oxides. At this high temperature, the dehydration rate was high enough that the intermediate, FAc-OH, was barely seen in the reaction profile as it dehydrated rapidly to FAc.

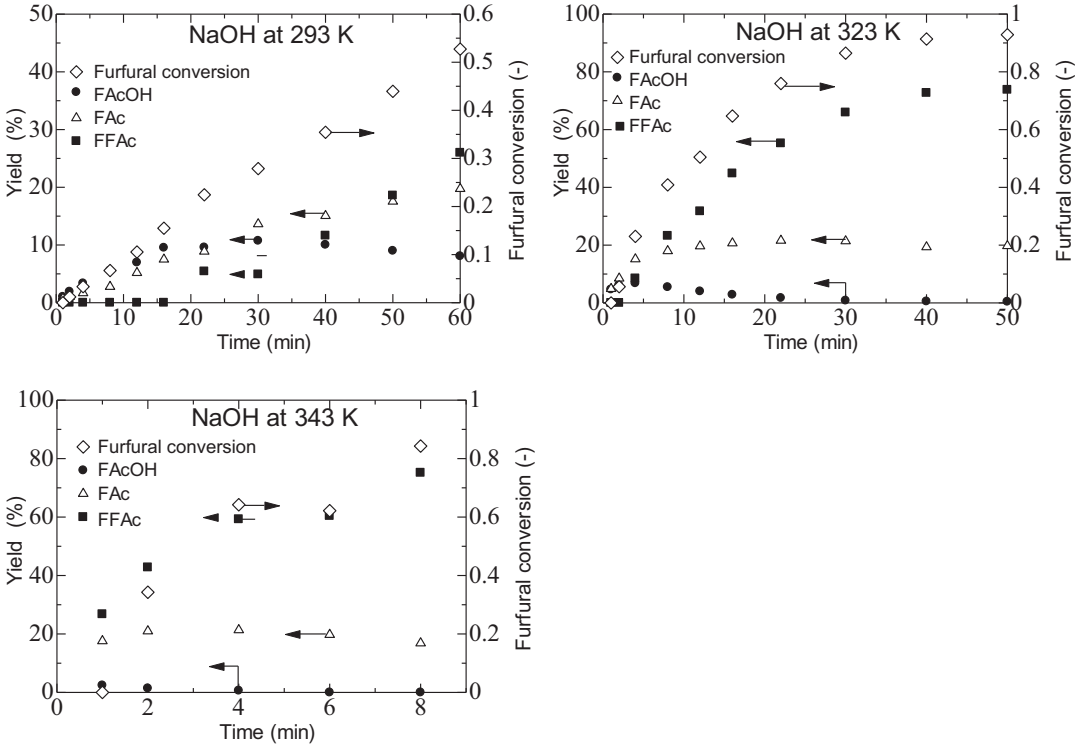


**Fig. 11.** Product yield and furfural conversion profiles with NaOH catalyst at 293, 323 and 343 K. (3.3 g acetone, 5.5 g furfural, 0.02 mole/L of NaOH, and 60 g of 1:1.5 (w/w) water and methanol solvent mixture).

### 3.4.2. Effect of water

Additional Brønsted sites that are accessible by *in situ* activation of calcined dolomite during the aldol condensation would avoid the time-consuming step of hydration. Fig. 12 shows conversion and yield profiles when calcined dolomite was used without a prior hydration step. Calcined dolomite was less active (surface basicity of 0.19 meq. $OH^-$/g), more affected by deactivation (confirmed by TPD and TPO results) and more selective to FFAC than hydrated dolomite. There is possibility therefore that the fast hydration mechanism at reaction temperature could cause breaking of dolomite particles of weak mechanical strength and large porous volume.

### 3.4.3. Reaction pathway

The kinetic model proposed here simplifies the mechanism proposed by West et al. [9] as a single liquid phase was used. The model is first applied to activated dolomite and then extended to NaOH catalyst. In addition, a step showing the formation and disappearance of the intermediate FAc-OH is taken into account in the kinetic mechanism. The chemical equilibrium was first investigated as water reacts not only with FAc and FFAc (Eqs. (5b and 5c)) and thus shifts the chemical equilibrium, but also with dolomite to produce hydroxyl basic sites. The equilibrium constants, $K_c$, of reactions (4a)–(4c) obtained at long residence time – ca. 12 h – and temperatures of 306, 323, 343, 373 and 413 K, using activated dolomite as illustrated in Fig. 13, confirm that unlike FAc-OH, intermediate dehydration (5b), furfural aldol-condensation and re-condensation (Eqs. (5a and 5c)) are exothermic as favoured at low temperatures. The values of the equilibrium constants, however, clearly show that a backward reaction is only feasible in the case of reaction (5a). Eqs. (5a)–(5c) are therefore:

$$F + Ac \overset{k_1/k_{-1}}{\leftrightarrow} \text{FAc-OH} \quad (7a)$$

$$\text{FAc-OH} \overset{k_2}{\rightarrow} \text{FAc} + \text{water} \quad (7b)$$

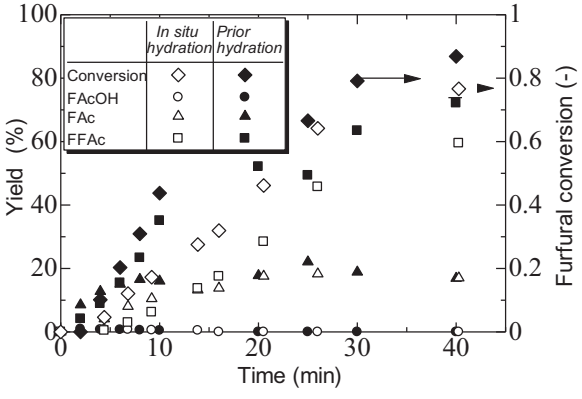


**Fig. 12.** Product yield and furfural conversion profiles with calcined and hydrated dolomite (full symbols) and calcined and *in situ* hydrated dolomite (open symbols) at 413 K, (3.3 g acetone, 5.5 g furfural, 0.5 g dolomite, and 60 g of 1:1.5 (w/w) water and methanol solvent mixture).

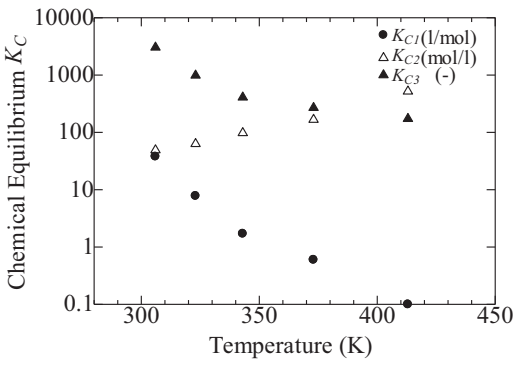


**Fig. 13.** Chemical equilibrium constants, $K_C$, profiles with temperature.

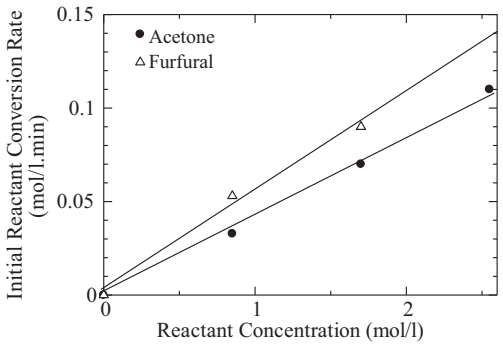


**Fig. 14.** Initial reactant rates vs. furfural and acetone concentrations (Temperature: 343 K, 0.5 g activated dolomite, and 60 g of 1:1.5 (w/w) water and methanol solvent mixture).

$$\mathrm{FAc} + \mathrm{F} \xrightarrow{k_3} \mathrm{FFAc} + \mathrm{water} \tag{7c}$$

The first step is the reaction of furfural and acetone to produce FAc-OH which further dehydrates to FAc. FAc reacts with furfural into FFAc due the symmetry of acetone molecule. Preliminary tests on effects of the initial concentrations of acetone and furfural on their initial rates of disappearance were investigated. Fig. 14 shows a linear increase of initial rates with initial concentrations, obtained by data extrapolation to the starting time, implying that aldol-condensation follows a kinetic of a pseudo-first order model with respect to the catalytic surface coverage of furfural and acetone on base sites of the calcined dolomite.

The reaction rate, $r_i$ based on hydroxyl ions, is therefore defined by Eq. (8) and explicitly extended to (Furfural) F, acetone (Ac), FAc-OH, FAc and FFAc, as illustrated by Eqs. (9a)–(9e). Deactivation by carbon deposits of activated dolomite was not considered in the kinetic model as the decrease in furfural conversion after reuse was observed at the highest temperatures (ca. 413 K).

$$r_i = \frac{dn_i}{m_{\mathrm{cat}} C_{\mathrm{OH}} dt} \tag{8}$$

$$r_F = -r_1 + r_{-1} - r_3 \tag{9a}$$

$$r_{Ac} = -r_1 + r_{-1} \tag{9b}$$

$$r_{\mathrm{FAc\text{-}OH}} = r_1 - r_{-1} - r_2 \tag{9c}$$

$$r_{\mathrm{FAc}} = r_2 - r_3 \tag{9d}$$

$$r_{FFAc} = r_3 \tag{9e}$$

Here, the value of the basicity, $C_{OH}$, of activated dolomite is taken as 0.72 meq. $OH^-$/g as mentioned in Section 3.1. The reaction rates $r_1$, $r_{-1}$, $r_2$, and $r_3$ are expressed in terms of the surface coverage, $\vartheta$, by Eq. (10a)–(10d) following Langmuir–Hinshelwood where each species occupies a single active site:

$$r_1 = k_1 \vartheta_{\mathrm{F}} \vartheta_{\mathrm{Ac}} \tag{10a}$$

$$r_{-1} = k_{-1} \vartheta_{\mathrm{FAc\text{-}OH}} \tag{10b}$$

$$r_2 = k_2 \vartheta_{\mathrm{FAc\text{-}OH}} \tag{10c}$$

$$r_3 = k_3 \vartheta_{\mathrm{F}} \vartheta_{\mathrm{FAc}} \tag{10d}$$

$$\vartheta_i = \frac{K_i}{1 + \sum_{j=1}^{n} K_j C_j} C_i \tag{10e}$$

The coverage of component $i$, $\vartheta_i$ was approximated by a linear adsorption model of the concentrations in the liquid phase as diluted concentrations were used

$$\vartheta_i = K_i C_i \tag{11}$$

where $K$ is the equilibrium adsorption constant. Eq. (10a)–(10d) are rewritten in terms of concentrations as follows:

$$r_1 = k'_1 C_{\mathrm{F}} C_{\mathrm{Ac}} \tag{12a}$$

$$r_{-1} = k'_{-1} C_{\mathrm{FAc\text{-}OH}} \tag{12b}$$

$$r_2 = k'_2 C_{\mathrm{FAc\text{-}OH}} \tag{12c}$$

$$r_3 = k'_3 C_{\mathrm{F}} C_{\mathrm{FAc}} \tag{12d}$$

With

$$k'_1 = k_1 K_{\mathrm{F}} K_{\mathrm{Ac}} \tag{13a}$$

$$k'_{-1} = k_{-1} K_{\mathrm{FAc\text{-}OH}} \tag{13b}$$

$$k'_2 = k_2 K_{\mathrm{FAc\text{-}OH}} \tag{13c}$$

$$k'_3 = k_3 K_{\mathrm{F}} K_{\mathrm{FAc}} \tag{13d}$$

Herein, the rate constants $k'_1$, $k'_{-1}$, $k'_2$, and $k'_3$ were obtained by fitting experimental data of activated dolomite to the surface model. Other intrinsic rate constants $k_1$, $k_{-1}$, $k_2$ and $k_3$ were deduced by fitting experimental data of NaOH catalyst to a power law model describing the aldol-condensation in a homogeneous liquid phase (Eqs. (14a)–(14d)).

$$r_1 = k_1 C_{\mathrm{F}} C_{\mathrm{Ac}} \tag{14a}$$

$$r_{-1} = k_{-1} C_{\mathrm{FAc\text{-}OH}} \tag{14b}$$

$$r_2 = k_2 C_{\mathrm{FAc\text{-}OH}} \tag{14c}$$

$$r_3 = k_3 C_{\mathrm{F}} C_{\mathrm{FAc}} \tag{14d}$$

### 3.4.4. Estimation of kinetic parameters

The rate constants $k'_1$, $k'_{-1}$, $k'_2$ and $k'_3$, and $k_1$, $k_{-1}$, $k_2$ and $k_3$ were determined by fitting the differential equations with the experimental data based on concentrations of activated dolomite and NaOH tests, respectively. The differential equations were solved using Runge–Kutta algorithm with a self-adjusting step. The rate constants were calculated by minimisation of the sum of squares of residuals using a non-linear least squares algorithm based on the Marquardt method to adjust the kinetic parameters. The data fits of the kinetic model at 323 K are illustrated by Fig. 7(a) and (b). The curves fit the model depicted in Fig. 8 reasonably well and the Arrhenius plots for activated dolomite catalyst are given in Fig. 15. The activation energies and pre-exponential factors of each reaction for both activated dolomite and NaOH catalysts are reported in Table 2. The activation energy for the formation of FFAc was low compared with other reactions. This explains why the selectivity to FFAC with activated dolomite is so prominent at high temperatures, accounting for the majority of products at the end of each reaction (<22.3 kJ/mol). The activation energy for the formation (ca. 39.4 kJ/mol) of FAc-OH from furfural and acetone was considerably lower than the one of the reverse reaction (ca. 51.0 kJ/mol) allowing the formation of FAc-OH intermediate to be sensitive to the operating temperatures. The kinetic model proposed with activated dolomite catalyst fits more data than NaOH catalyst with a normalised standard deviation (NSD) of 2.0% when compared with activated dolomite (ca. NSD of 6.2%) as illustrated in Table 2.

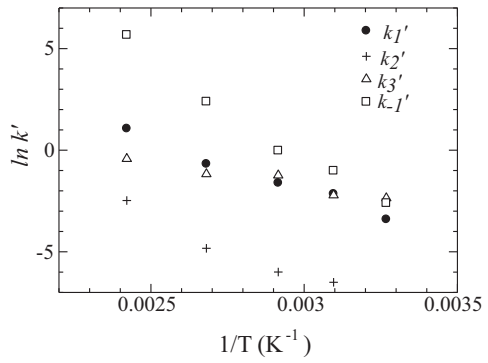


**Fig. 15.** Arrhenius Plot of the rate constants.

**Table 2**
Rate and adsorption constants.

| Reaction constant | Activation energy (kJ/mol) | | Arrhenius constant | |
|---|---|---|---|---|
| | $E_{dolomite}$ | $E_{NaOH}$ | $A_{0dolomite}$ | $A_{0NaOH}$ |
| $k'_1$ [$m^6$/mol.eq. $OH^-$ s] | 39.4 | – | $270 \times 10^3$ | – |
| $k'_2$ [$m^3$/eq. $OH^-$ s] | 50.2 | – | $382 \times 10^5$ | – |
| $k'_3$ [$m^6$/mol.eq. $OH^-$.sec] | 22.3 | – | 162 | – |
| $k'_{-1}$ [$m^3$/eq. $OH^-$ s] | 51.0 | – | $2.1 \times 10^6$ | – |
| $k_1$ [$m^6$/mol.eq. $OH^-$ s] | – | 55.8 | – | $865 \times 10^3$ |
| $k_2$ [$m^3$/eq. $OH^-$ s] | – | 70.8 | – | $196 \times 10^9$ |
| $k_3$ [$m^6$/mol.eq. $OH^-$ s] | – | 55.6 | – | $196 \times 10^6$ |
| $k_{-1}$ [$m^3$/eq. $OH^-$ s] | – | 70.6 | – | $845 \times 10^7$ |

| Adsorption constant | Adsorption enthalpy (kJ/mol) |
|---|---|
| $\Delta H_{FAc\text{-}OH}$ | −20.6 |
| $\Delta H_{Ac} - \Delta H_{FAc}$ | 16.9 |

NSD for dolomite: furfural: 3.64, acetone: 4.83%, FAc-OH: 12.15%, FAc: 4.16%, FFAc: 6.31% and average: 6.21%.
NSD for NaOH: furfural: 1.98, Acetone: 1.63%, FAc-OH: 1.65%, FAc: 2.86%, FFAc: 1.85% and average: 2.00%.

This lower approximation could be due to assumption of linear adsorption on activated dolomite (Eq. (10)). The better selectivity of activated dolomite towards the second condensation (FFAc) is clearly illustrated with adsorption enthalpy of FAc 16.9 kJ/mol higher than its competitor acetone.

## 4. Conclusions

This work aimed to use activated dolomite as a potential catalyst for aldol-condensation of furfural. The activation was carried out by successive calcination and hydration steps allowing creation of an unchanged number of active base sites for aldol-condensation for further kinetic modelling. The structure of the dolomite was found to change during the dolomite preparation, i.e. via calcination and hydration, producing highly catalytically active material. On charring dolomite for 8 h at 1073 K, complete decomposition was achieved causing calcium carbonate and magnesium carbonate to break down into their oxides whilst releasing carbon dioxide. These results were confirmed by XRD analysis, which showed that the carbonate component had disappeared and was replaced by oxides. Calcination not only changed the chemical composition, but also altered the physical structure of the dolomite by causing ruptures and stresses, and resulting in more porous materials after the release of $CO_2$. These results were also confirmed by SEM analysis which displayed the changes on flat, angular plains of uncalcined dolomite into a spongy, almost pumice like appearance, with an increase in the surface area from 3.2 to 13.2 $m^2$/g. The structure of the calcined dolomite changed further when mixed with a water–methanol solution by producing calcium and magnesium hydroxides with an increase in the surface area from 13.2 to 25.0 $m^2$/g and in the basicity from 0.31 to 0.72 meq. $OH^-$/g.

The power law model of kinetics first-order with respect to acetone and furfural fitted well actual experimental data with a normalised standard deviation of 6.2% for activated dolomite and 2.0% for NaOH catalyst. The reaction mechanism in a single phase of water–methanol solution began with the deprotonation of acetone forming a carbanion intermediate, which then reacted with the carbonyl group of furfural to form a water soluble $C_8$ FAc-OH monomer. FAc-OH readily dehydrated to form $C_8$ FAc monomer, which reacted with furfural to form $C_{13}$ FFAc dimer. Sodium hydroxide was more selective towards lumped FAc monomer and FFAc dimer compared with activated dolomite which has shown carbon losses and deactivation, particularly at high temperatures. Activated dolomite was more selective to the re-condensation (FFAc dimer) owing to adsorption enthalpy on activated dolomite of FAc monomer which was found higher than acetone. Modified dolomites are therefore promising catalysts to produce $C_{13}$ dimers which can be transformed upon hydrogenation and deep hydrodeoxygenation in high-quality diesel fuels.

## Acknowledgement

This work was supported by the Department of education and Learning, Northern Ireland, United Kingdom.

## Appendix A. Supplementary data

Supplementary data associated with this article can be found, in the online version, at http://dx.doi.org/10.1016/j.apcatb.2013.07.006.

## References

[1] G.A. Florides, P. Christodoulides, Environment International 35 (2009) 390–401.
[2] F. Cherubini, A.H. Strmman, Biofuels, Bioproducts and Biorefining 5 (2011) 548–561.
[3] J.N. Chheda, J.A. Dumesic, Catalysis Today 123 (2007) 59–70.
[4] R. O'Neil, M.N. Ahmad, L. Vanoye, F. Aiouache, Industrial & Engineering Chemistry Research 48 (2009) 4300–4306.
[5] W. Xie, Y. Liu, H. Chun, Catalysis Letters 142 (2012) 352–359.
[6] W. Shen, G.A. Tompsett, K.D. Hammond, R. Xing, F. Dogan, C.P. Grey, W.C. Conner, S.M. Auerbach, G.W. Huber, Applied Catalysis A-General 392 (2011) 57–68.
[7] I. Sadaba, M. Ojeda, R. Mariscal, J.L. Fierro, M.L. Granados, Applied Catalysis B: Environmental 101 (2011) 638–648.
[8] N. Fakhfakh, P. Cognet, M. Cabassud, Y. Lucchese, Chemical Engineering and Processing: Process Intensification 47 (2008) 349–362.
[9] R.M. West, Z.Y. Liu, M. Peter, Journal of Molecular Catalysis A: Chemical 296 (2008) 18–27.
[10] G.W. Huber, J.N. Chheda, C.J. Barrett, J.A. Dumesic, Science 308 (2005) 1446–1450.
[11] R. Xing, A. Subrahmanyam, H. Olcay, W. Qi, G. van Walsum, H. Pends, G.W. Huber, Green Chemistry 12 (2010) 1933–1946.
[12] I. Cota, I.E. Ramirez, F. Medina, J.E. Sueiras, G. Layrac, D. Tichit, Applied Clay Science 50 (2010) 498–502.
[13] H. Liu, W. Xu, X. Liu, Y. Guo, Y. Guo, G. Lu, Y. Wang, Kinetics and Catalysis 51 (2010) 75–80.
[14] M.L. Kantam, B.M. Choudary, C.V. Reddy, K.K. Rao, F. Figuéras, Chemical Communications 9 (1998) 1033–1034.
[15] M.J. Climent, A. Corma, S. Iborra, A. Velty, Journal of Molecular Catalysis 182/183 (2002) 327–342.
[16] M.J. Climent, A. Corma, S. Iborra, A. Velty, Catalysis Letters 79 (2002) 157–163.
[17] J.C.C.A.A. Roelofs, A.J. van Dillen, K.P. de Jong, Catalysis Today 60 (2000) 297–303.
[18] K.K. Rao, M. Gravelle, S. Valente, F.J. Fuguéras, Journal of Catalysis 173 (1998) 115–121.
[19] D. Tichit, B. Coq, S. Cernaux, R. Durand, Catalysis Today 75 (2002) 197–202.
[20] A. Guida, M.H. Lhouty, D. Tichit, F. Figueras, Applied Catalysis A-General 164 (1997) 251.
[21] B. Yoosuk, P. Udomsap, B. Puttasawat, Applied Catalysis A-General 395 (2011) 87–94.
[22] K. Wilson, C. Hardacre, Green Chemistry 10 (2008) 654–659.

[23] S. Abello, D. Vijaya-Shankar, J. Perez-Ramirez, Applied Catalysis A-General 342 (2008) 119–125.
[24] P. Staszczuk, E. Stefaniak, B. Bilinski, E. Szymanski, R. Dobrowolski, S.A.A. Jayaweera, Powder Technology 92 (1997) 253–257.
[25] A. Duffy, G.M. Walker, S. Allen, Chemical Engineering Journal 117 (2006) 239–244.
[26] L. Faba, E. Diaz, S. Ordonez, Applied Catalysis B: Environmental 113/114 (2012) 201–211.
[27] E. Kang, D.W. Chae, B. Kim, Y.G. Kim, Journal of Industrial and Engineering Chemistry 18 (2012) 174–177.
[28] G. Chamoulaud, D. Floner, C. Moinet, C. Lamy, C.E.M. Belgsir, Electrochimica Acta 46 (2001) 2757–2760.
[29] S. Tsunetake, H. Hideshi, S. Tishchenko, Catalysis Surveys from Asia 7 (2003) 145–156.
[30] G.G. Podrebarac, F.T.T. Ng, G.L. Rempel, Chemical Engineering Science 52 (1997) 2991–3002.
[31] R. Roque-Malherbe, J. de Onate-Martinez, E. Navarro, Journal of Materials Science Letters 12 (1993) 1037–1038.